Modeling, Simulation and Comparison of Control Techniques for Energy Storage Systems

Álvaro Ortega, *Student Member, IEEE*, Federico Milano, *Fellow, IEEE*

Abstract— This paper describes the modeling and formulation of a variety of deterministic techniques for energy storage devices, namely the PI, H-infinity and sliding mode controllers. These techniques are defined based on a general, yet detailed, energy storage device model, which is accurate for transient stability analysis. The paper also presents a thorough statistical comparison of the performance and robustness of the considered control techniques, using stochastic dynamic models and a variety of disturbances and scenarios. The case study is based on a 1,479-bus model of the all-island Irish transmission system and an energy storage device actually installed in the system.

Index Terms— Energy storage system, robust control, stochastic differential-algebraic equations, Monte Carlo method.

I. INTRODUCTION

A. Motivation

The increasing penetration of non-dispatchable generation, typically based on renewable energy resources, has consistently threatened the stability of power systems. This kind of generation, in fact, is non-synchronous, i.e., does not provide inertia, and its energy resources tend to be both uncertain and volatile. Energy Storage Systems (ESSs) can play an important role in improving the dynamic response of the power system and mitigating the issues above. For example, ESSs can help regulate the active power supplied by non-dispatchable generation and provide primary frequency and voltage control. The flexibility and versatility of ESSs has motivated the growth of a variety of energy storage technologies, such as batteries, flywheels, super-capacitors, etc., as well as control strategies aimed at optimizing the performance of ESSs [1], [2]. The aim of this paper is to exhaustively compare different energy storage technologies and control strategies considering a real-world hybrid flywheel and battery energy storage system.

B. Literature Review

The best known and most commonly used ESS control technique is the PI-based controller [3], [4] but other, more sophisticated and robust controllers have been proposed in the literature. These can be deterministic and, typically, model-dependent, e.g., H-infinity (H_∞) control [5], [6], sliding mode (SM) control [7]–[9], model predictive control [10], [11], or based on heuristics, such as fuzzy logic control [12]. These references show the advantages of robust techniques with respect to the PI controller. However, the focus is only on a specific energy storage technology and a given system operating condition. Moreover, the references above

Á. Ortega and F. Milano are with the School of Electrical and Electronic Engineering of the University College Dublin, Belfield, Ireland.
(e-mails: alvaro.ortega-manjavacas@ucdconnect.ie; federico.milano@ucd.ie).

do not consider real-world applications. To the best of our knowledge, there is no work aimed at classifying, through a comprehensive stochastic approach, the dynamic behavior of each control technique considering different ESS technologies, contingencies and system scenarios. The aim of this paper is to fill this gap.

One of the main difficulties involved in achieving the goal of the paper is the wide variety of available energy storage technologies, which complicates the implementation and design of the controllers, in particular, for techniques that are strongly model-dependent, e.g., H_∞ and SM. To solve this issue, without compromising the fidelity of the simulations, we use the Generalized ESS Model (GEM) that we proposed in [13]. An interesting property of the GEM model is to retain the physical meaning of the main energy quantities, i.e., potential and flow variables. In the paper, we show that, thanks to this property, the model proposed in [13] proves to be particularly suited to being coupled with robust controllers such as the H_∞ and SM. Preliminary results on the performance of the GEM coupled with different control strategies are presented in [14].

C. Contributions

The paper recalls the main features of three control techniques, namely, PI, H_∞ and SM and describes the formulation of such techniques above based on the GEM.

Then, the paper presents an exhaustive comparison of the robustness of the dynamic response the ESS controllers based on PI, H_∞ and SM techniques. With this aim, uncertainties related to both generation and demand, different loading levels and contingencies, i.e., faults and line and generator outages, are considered. Both ESS active power and frequency regulations are studied considering all the above.

All comparisons are based on a Monte Carlo method applied to a 1,479-bus model of the Irish transmission grid with an existing Hybrid ESS (HESS), that is composed of a Flywheel Energy Storage (FES) and a Battery Energy Storage (BES) device. The grid model is formulated as a set of stochastic differential-algebraic equations as discussed in [15].

D. Paper Organization

The remainder of this paper is organized as follows. The general scheme of a Voltage Sourced Converter (VSC)-based ESS, as well as the formulation of the GEM are presented in Section II. Section III describes the PI, H_∞ and SM controllers, and how to set them up with the GEM. Section IV discusses the case study based on the all-island Irish transmission system. Conclusions are drawn in Section V.
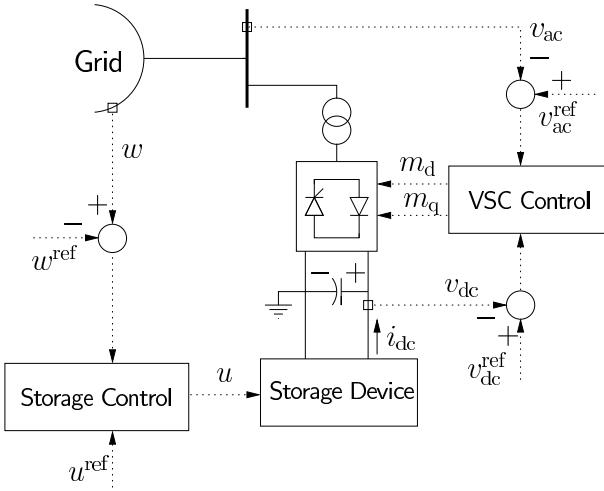
Fig. 1: VSC-based ESS coupled to the grid.

II. Configuration of the Energy Storage System

The configuration of the ESS utilized in this paper includes a storage device, a VSC converter, and their respective controllers (see Fig. 1). The state of the art dq-frame VSC model described in [16], which includes PI current controllers and limiters, is used in this paper. Then, the GEM that is proposed in [13] is used for representing the dynamic behavior of the storage device. This model represents two properties that are relevant for the synthesis of the controllers discussed in Section III: (i) a linear time-invariant structure, and (ii) a fixed number of variables and equations, independent of the storage technology. Moreover, as shown in [13], the GEM approximates detailed ESS models with greater fidelity than other excessively simplified models that have been proposed in the literature.

For completeness, the main steps and assumptions to define the GEM are briefly outlined in the remainder of this section. The starting point is the linearized, technology-dependent, expression of the storage device model under study:

$$\begin{aligned} \mathbf{T}_x \dot{\boldsymbol{x}} &= \mathbf{A}_{xx} \boldsymbol{x} + \mathbf{A}_{xz} \boldsymbol{z} + \mathbf{B}_{xu} u + \mathbf{B}_{xv} v_{\mathrm{dc}} + \mathbf{K}_x \\ \mathbf{T}_z \dot{\boldsymbol{z}} &= \mathbf{A}_{zx} \boldsymbol{x} + \mathbf{A}_{zz} \boldsymbol{z} + \mathbf{B}_{zu} u + \mathbf{B}_{zv} v_{\mathrm{dc}} + \mathbf{K}_z \\ i_{\mathrm{dc}} &= \mathbf{C}_x \boldsymbol{x} + \mathbf{C}_z \boldsymbol{z} + \mathrm{D}_u u + \mathrm{D}_v v_{\mathrm{dc}} + \mathrm{K}_i \end{aligned} \quad (1)$$

where the state vector $\boldsymbol{x}$ are the potential and flow variables related to the energy stored in the ESS, and $\boldsymbol{z}$ stands for all other variables; u is the output signal of the storage control; v_{dc} and i_{dc} are the dc voltage and current of the VSC, respectively. Note that (1) is expressed using the semi-implicit formulation presented in [17]. Therefore, $\mathbf{T}_x$ and $\mathbf{T}_z$ are time-invariant, not necessarily diagonal nor full-rank matrices. Note also that u, v_{dc} and i_{dc} are scalar, whereas all other quantities are vectors. Equation (1) is written for $\boldsymbol{x}$, $\boldsymbol{z}$, u, v_{dc} and i_{dc}, not the incremental values $\Delta \boldsymbol{x}$, $\Delta \boldsymbol{z}$, Δu, Δv_{dc} and Δi_{dc}. With this aim, $\mathbf{K}_x$, $\mathbf{K}_z$ and K_i account for the values of the variables at the equilibrium point.

The dynamic order of (1) is reduced, assuming that the dynamics of the variables in $\boldsymbol{z}$ are adequately faster than those of $\boldsymbol{x}$ (i.e., $\mathbf{T}_z \dot{\boldsymbol{z}} = \mathbf{0}$). Therefore, after computing the Schur components of $\boldsymbol{z}$, and rewriting the matrices in compact form,

TABLE I: Potential and flow variables of different energy storage devices.

Storage Device	Potential	Flow
Super-conducting Coil	Magneto Motive Force	Flux
Compressed Air Tank	Pressure	Mass Flow
Super-capacitor	Voltage	Electric Current
Battery	Electrochem. Potential	Molar Flow Rate
Flywheel	Angular Speed	Torque

the following set of three DAEs is obtained:

$$\begin{aligned} \mathbf{T}_x \dot{\boldsymbol{x}} &= \tilde{\mathbf{A}} \boldsymbol{x} + \tilde{\mathbf{B}}_u u + \tilde{\mathbf{B}}_v v_{\mathrm{dc}} + \tilde{\mathbf{K}}_x \quad (2) \\ i_{\mathrm{dc}} &= \tilde{\mathbf{C}} \boldsymbol{x} + \tilde{\mathrm{D}}_u u + \tilde{\mathrm{D}}_v v_{\mathrm{dc}} + \tilde{\mathrm{K}}_i \end{aligned}$$

where, for example, the matrix $\tilde{\mathbf{A}}$ is computed as follows:

$$\tilde{\mathbf{A}} = \mathbf{A}_{xx} - \mathbf{A}_{xz} \mathbf{A}_{zz}^{-1} \mathbf{A}_{zx} \quad (3)$$

where the non-singularity of matrix $\mathbf{A}_{zz}$ is assumed. Other matrices and scalars in (2) are computed in a similar way to in (3). It is important to note that the vector $\boldsymbol{x}$ is selected in such a way that it always contains, at least, two variables, say x_1 and x_2, that represent a *potential* and a *flow*. This is clearly always possible, independently of the ESS technology that is employed (see Table I).

Finally, the energy stored in the device is computed as:

$$E = \sum_{i=1}^{n} \rho_i \left(x_i^{\beta_i} - \chi_i^{\beta_i} \right) \quad (4)$$

where ρ_i, β_i and χ_i are the proportional and exponential coefficients, and the reference value of x_i, respectively. Note that ρ_i coefficient is non-null only if x_i represents a flow or potential quantity of the ESS.

Detailed transient stability models of FES and BES, and the derivation of the GEM for these technologies are presented in Appendices I and II, respectively.

III. Control Strategies for ESSs

This section presents the ESS control techniques considered in the case study of this paper, namely, the PI, H_∞ and SM. The main features of these strategies are outlined and discussed, and the formulations of the H_∞ and SM controllers for the GEM are also described.

In the following, we assume that ESS parameters and other relevant data are available (e.g., are provided by manufacturers). These data are embedded in detailed ESS models and, based on that, the parameters of the GEM in (2) are calculated (see [13] for some examples of this procedure). Then, the control strategies are implemented and designed based on the GEM. Note that, if necessary, the designed controller can be applied to the original detailed ESS model without modification, which is, in our opinion, one of the main advantages of using the GEM formulation.

A. PI Control

Figure 2 depicts a typical ESS PI controller scheme. This configuration includes a dead-band and a low-pass filter, a PI regulator, and a storage input limiter aimed to attenuate the effect of transients derived from energy saturations of the ESS [18].
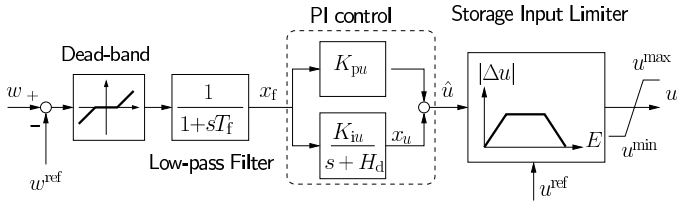
Fig. 2: PI-based control for ESSs.

The PI regulator is composed of a proportional gain, K_{pu}, and an integrator with gain K_{iu} and integral deviation coefficient H_d. These parameters are commonly tuned by trial-and-error or pole-placement techniques. The simplicity of the implementation and design, as well as the mass utilization of this controller in industrial applications are its main strengths. Note also that the structure of the PI does not depend on the energy storage technology considered. However, it has been shown that system uncertainties and topological changes can significantly deteriorate the behavior of this controller, and thus of the entire system [9]. This justifies the need for the development of more sophisticated and robust controllers, such as the ones that are described in the remainder of this section.

B. H∞ Control

The main objective of any optimal control approach consists of synthesizing a controller such that the closed-loop system is stable, and the performance output is minimized, given a class of disturbance inputs. Since the minimization of the energy gain of the closed-loop system can be too complicated to achieve in practice, the H∞ approximates the solution of the problem above by minimizing the H∞ norm of the closed-loop transfer function of the system shown in Fig. 3 [5], [6], [19]. Even considering only a linear time-invariant system, the synthesis of a H∞ controller is challenging, as input and output quantities have to be chosen with care.
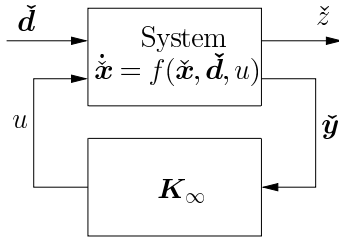

Fig. 3: H∞ controller.

With this aim, the relevance of the fixed and linear structure of the GEM outlined in the previous section becomes apparent. In fact, since the vector x always includes potential and flow quantities, which can be used to determine the overall energy of the ESS, it is relatively simple to set up a linear controller K_∞. Using similar notation to that in (2), the equations of the upper block in Fig. 3 are:

$$\check{\mathbf{T}}_x \dot{\check{x}} = \check{\mathbf{A}} \check{x} + \check{\mathbf{B}}_1 \check{d} + \check{\mathbf{B}}_2 u$$
$$\check{z} = \check{\mathbf{C}}_1 \check{x} + \check{\mathbf{D}}_{11} \check{d} + \check{\mathbf{D}}_{12} u \quad (5)$$
$$\check{y} = \check{\mathbf{C}}_2 \check{x} + \check{\mathbf{D}}_{21} \check{d} + \check{\mathbf{D}}_{22} u$$

where:

- $\check{x} = [x_1 \ x_2 \ x_u]^T$, where x_1 and x_2 are the state variables of the system in (2); and x_u is the output of the integrator in Fig. 2;
- $\check{\mathbf{T}}_x = \begin{bmatrix} \mathbf{T}_x & \mathbf{0} \\ \mathbf{0} & 1 \end{bmatrix}$;
- $\check{d} = [x_f \ v_{dc}]^T$ are the external perturbations;
- $\check{z} = x_u - K_u u$ is the regulated output signal. K_u is a positive weight coefficient to couple the output of the PI controller and the converter of the storage device.
- $\check{y} = [\hat{u} \ v_{dc}]^T$ are the measurement outputs of the system.

Note that the inclusion of the output of the integrator, x_u, in the state vector of (5) allows implementing a droop frequency control through the ESS (if $H_d \neq 0$ in the control scheme of Fig. 2).

The synthesis of a H∞ controller requires that a set of well posedness constraints are satisfied, as follows:

i. $(\check{\mathbf{A}}, \check{\mathbf{B}}_2)$ is stabilizable;
ii. $(\check{\mathbf{C}}_2, \check{\mathbf{A}})$ is detectable;
iii. $\check{\mathbf{D}}_{11} = \mathbf{0}$ and $\check{\mathbf{D}}_{22} = \mathbf{0}$;
iv. $\text{rank}[\check{\mathbf{D}}_{12}] = \dim u = 1$, i.e., $\check{\mathbf{D}}_{21}$ must be left invertible (full control penalty);
v. $\text{rank}[\check{\mathbf{D}}_{21}] = \dim \check{y} = 2$, i.e., $\check{\mathbf{D}}_{21}$ must be right invertible (full measurement noise);
vi. $\text{rank}\begin{bmatrix} j\omega\mathbf{I}_3 - \check{\mathbf{A}} & \check{\mathbf{B}}_2 \\ \check{\mathbf{C}}_1 & \check{\mathbf{D}}_{12} \end{bmatrix} = \dim \check{x} + \dim u = 4$,

for all real ω;

vii. $\text{rank}\begin{bmatrix} j\omega\mathbf{I}_3 - \check{\mathbf{A}} & \check{\mathbf{B}}_1 \\ \check{\mathbf{C}}_2 & \check{\mathbf{D}}_{21} \end{bmatrix} = \dim \check{x} + \dim \check{y} = 5$,

for all real ω.

Conditions iv to vii impose that the problem is not singular. If (5) satisfies all conditions above, then a suboptimal solution for K_∞ can be found by solving two algebraic Riccati equations, which have same order as the original system to be controlled.[1] The structure of the resulting controller indicated as K_∞ in Fig. 3 is as follows:

$$\dot{x}_\infty = \mathbf{A}_\infty x_\infty + \mathbf{B}_\infty \check{y}$$
$$u = \mathbf{C}_\infty x_\infty + \mathbf{D}_\infty \check{y} \quad (6)$$

It is important to note that the H∞ problem is formulated for an augmented model of the GEM, i.e., (5) and that it does not involve nor require the knowledge of the dynamics of the whole transmission system. This fact makes feasible the implementation of (5)-(6) in real-world applications.

C. Sliding Mode Control

The basic principle of the SM control is to take advantage of a switching control logic to force the trajectories of a dynamic variable-structure system to follow a given path, called *sliding surface*. If the sliding surface, say $\mathcal{S}$, satisfies usual requirements of existence and reachability, which in turn are needed to satisfy Lyapunov asymptotic stability conditions, the motion associated with the SM control is robust against

---

[1]In the case study, the Fortran library SLICOT is used to solve Riccati equations [20].

disturbances [21]. Due to the switching logic requirements, natural targets for SM controllers are devices that include power electronic converters and, with regard to ESSs, it has been proposed for the control of super-capacitor energy storage devices [7] and FESs [8].

The SM control also shows some drawbacks. The switching logic, in fact, is prone to produce the *chattering* effect (see Fig. 4), which is a persistent high-frequency periodic motions around the sliding surface $\mathcal{S}$ and is caused by the deviation of the real system from the ideal model. Typical, inevitable causes of the chattering are small control delays, hysteresis and deadbands of physical devices. Moreover, since the SM control is a model-dependent technique, its implementation for non-linear systems is often a challenge.
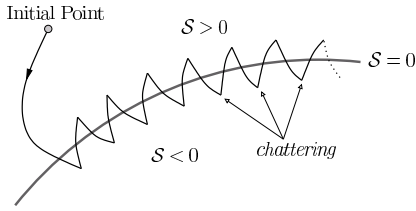

Fig. 4: Graphical representation of the dynamic behavior of a sliding control. Note the chattering effect arising once the trajectory of the variable reaches the sliding surface $\mathcal{S}$.

The linear structure of the GEM summarized in Section II highly simplifies the implementation of SM on ESSs. The discontinuous output signal of the storage control, u, can be rewritten as the sum of two terms, as follows:

$$u = u_{\mathrm{eq}} - K_{\mathrm{SM}} \operatorname{sign}(\mathcal{S}) \qquad (7)$$

where u_{eq} is the continuous component of the control during the sliding mode operation; and K_{SM} is a positive gain designed to reduce the effect of external perturbations and disturbances.

Since the variables x_1 and x_2 of the GEM in (2) have the meaning of a potential and a flow, the following equation is a good candidate for the sliding surface $\mathcal{S}$:

$$\mathcal{S} = x_{\mathrm{f}} - s_{x_{12}} x_1 x_2 \qquad (8)$$

where $x_1 x_2$ has the unit of a power; x_{f} is the filtered deviation of the measured signal w to be regulated (see Fig. 2); and $s_{x_{12}}$ is a coefficient that accounts for the unit of the variables in $\mathcal{S}$.

Linearizing (8) around the equilibrium point for which the GEM in (2) is obtained:

$$(\mathcal{S} - \mathcal{S}_0) = (x_{\mathrm{f}} - x_{\mathrm{f}0}) - s_{x_{12}} \left[x_{20}(x_1 - x_{10}) + x_{10}(x_2 - x_{20}) \right] \qquad (9)$$

At the equilibrium point, $\mathcal{S}_0 = 0$ and $x_{\mathrm{f}0} = 0$. Therefore:

$$\mathcal{S} = x_{\mathrm{f}} + s_x(x - x_0) \qquad (10)$$

where $s_x = - [s_{x_{12}} x_{20}, \ s_{x_{12}} x_{10}]$. If, at a given time t_{SM}, the trajectory falls on the sliding surface and $\dot{\mathcal{S}} = 0$, then $\mathcal{S} = 0$ for $t > t_{\mathrm{SM}}$. Moreover, $\dot{x}_{\mathrm{f}} = 0$ must hold during sliding mode. Hence, the derivative of (10) with respect to time is given by:

$$\dot{\mathcal{S}} = \dot{x}_{\mathrm{f}} + s_x \dot{x} = s_x \dot{x} = 0 \qquad (11)$$

and, from (2), one has:

$$\dot{\mathcal{S}} = s_x \mathbf{T}_x^{-1} [\tilde{\mathbf{A}} x + \tilde{\mathbf{B}}_u u + \tilde{\mathbf{B}}_v v_{\mathrm{dc}} + \tilde{\mathbf{K}}_x] = 0 \qquad (12)$$

Equation (12) allows the continuous component of the control u_{eq} to be defined as follows:

$$u_{\mathrm{eq}} = -(s_x \mathbf{T}_x^{-1} \tilde{\mathbf{B}}_u)^{-1} s_x \mathbf{T}_x^{-1} [\tilde{\mathbf{A}} x + \tilde{\mathbf{B}}_v v_{\mathrm{dc}} + \tilde{\mathbf{K}}_x] \qquad (13)$$

Therefore, SM can be applied to the ESS if $s_x \mathbf{T}_x^{-1} \tilde{\mathbf{B}}_u \neq 0$. If any variable $x_i \in x$ is algebraic, i.e., $\mathbf{T}_{x,\mathrm{ii}} = 0$, $\mathbf{T}_x^{-1}$ is not defined. A possible solution is to use the singular perturbation approach, i.e., assign $\mathbf{T}_{x,\mathrm{ii}} = \epsilon$, with $0 < \epsilon \ll 1$, or pass such a variable through a low-pass filter.

IV. CASE STUDY

In this section, the all-island Irish transmission system is utilized to compare the dynamic behavior of the ESS controllers described in the previous section. The topology and the steady-state data of the system are based on the actual real-world system provided by the Irish TSO, EirGrid. However, all dynamic data are estimated based on the knowledge of the various power plant technologies used. The dynamic model of the Irish system includes both conventional and wind power generation. The system consists of 1,479 buses, 1,851 transmission lines and transformers, 245 loads, 22 conventional synchronous power plants modeled with 6th order synchronous machine models with AVRs and turbine governors, 6 PSSs and 176 wind power plants, of which 142 are equipped with doubly-fed induction generators (DFIG) and 34 with constant-speed (CSWT).

The following remarks on the all-island Irish system are relevant:

- Wind power plants do not provide primary frequency regulation, as it occurs in the actual Irish system.
- The wind speed profile of each wind power plant is modeled as an uncorrelated Weibull distribution as in [22].
- Stochastic load variations are taken into account and modeled using Ornstein-Uhlenbeck processes [15], [23], [24].

In 2015, the company Schwungrad Energie installed a pilot HESS in a site close to Rhode, county Offaly, Ireland, [25], consisting of a BES and a FES. The installation is still a prototype and currently not complete but the ultimate goal is to use the HESS to provide primary frequency regulation and/or regulate the active power flowing through a high voltage transmission line physically close to the HESS.[2] The details of the regulations provided by the HESS have still to be agreed with the TSO [27], [28]. The power rating of the fully-operative HESS is expected to be about 20−30 MW. The FES will be responsible for filtering fast transients (e.g., 1 minute) due to its speed of response, while the BES will provide active power reserves over longer periods (e.g., 15 minutes) thanks to its higher energy capacity and power rate.

For the purposes of this case study, a HESS composed of a 50 MW BES and a 20 MW FES is assumed to be installed at a bus representing the town of Rhode. Note that the size

---

[2]The map of the Irish transmission system can be found online in [26].

of the HESS is larger than those that are currently installed in practice. By increasing the size of the HESS, the system level impacts of the HESS dynamics can be better appreciated. Moreover, it is expected that the size of these devices will increase substantially in the near future.

The case study presented in this section considers both active power flow and frequency regulation of the ESS, stochastic variations of both the wind and the loads, different system loading levels, and a variety of large disturbances such as faults followed by line outages, and the loss of generation units. The size of the grid, and the variety of scenarios considered in this section are designed to provide a fair and exhaustive comparison of the control techniques described in Section III, in terms of performance against contingencies and disturbances, robustness against system uncertainties, computational burdens and possible numerical/technical issues, such as saturations.

This section is organized as follows. Subsection IV-A compares the performance of the HESS controllers providing line active power control following the clearing of a three-phase fault and line disconnection. Subsection IV-B assumes that the HESS provides primary frequency control and considers the outage of a synchronous machine of the system.

To solve stochastic differential-algebraic equations, we use the Monte Carlo method. With this aim, 1,000 time domain simulations are carried out for each case. Each simulation is solved for 20 s in Subsection IV-A, and for 25 s in Subsection IV-B, with a time step of 0.004 s when SM is applied, and 0.02 s otherwise. Note that, for the considered time scale, the response of the BES is too slow for the SM to be effective and, hence, only the FES is regulated with the SM, while the H_∞ is applied to the BES. Finally, again for the considered time scale, the energy saturations of the HESS are neglected.

All simulations are obtained using Dome, a Python-based power system software tool [29]. The Dome version utilized in this case study is based on Python 3.4.1; ATLAS 3.10.1 for dense vector and matrix operations; CVXOPT 1.1.8 for sparse matrix operations; and KLU 1.3.2 for sparse matrix factorization. All simulations were executed on a server mounting 40 CPUs and running a 64-bit Linux OS.

A. Line Active Power Flow Regulation

In this subsection, we assume that the control of the HESS is designed to regulate P_{line}, the active power flowing through a high voltage transmission line of the Irish system, at 55 MW. We simulate a three-phase fault near the regulated line occurring at $t = 15$ s. This is then cleared by means of the disconnection of a transmission line after 180 ms. Note that $t = 15$ s is chosen to make sure that the stochastic processes of the wind and the load are in stationary conditions.

For fair comparison, the PI is tuned in order to obtain as similar performance as possible to the H_∞ and SM controllers, as shown in Fig. 5.a for a single trajectory. As an example of the HESS performance, the active power provided/consumed by the FES with each controller is shown in Fig. 5.b. Positive power indicates charging periods.
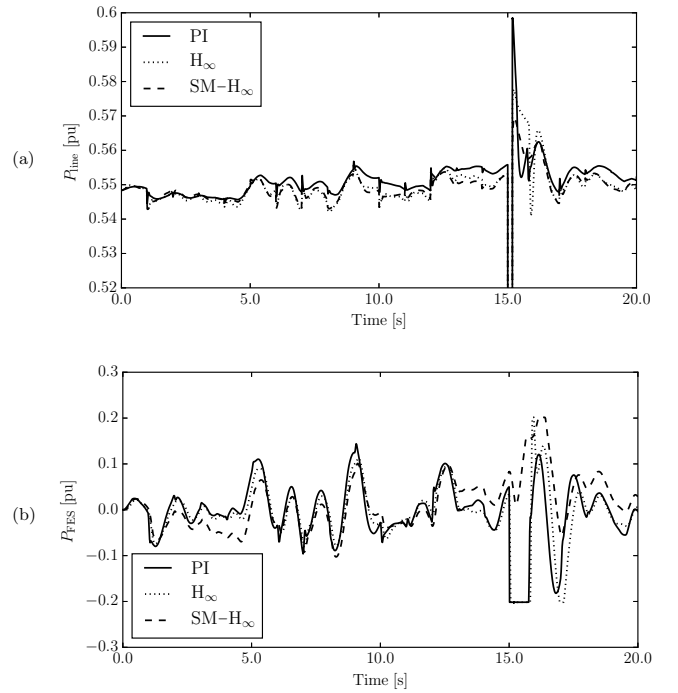

Fig. 5: Irish system with HESS and a three-phase fault followed by a line trip. (a) Power flowing through the regulated line; (b) Active power provided/consumed by the FES.

In the following, three different cases are considered: a base case loading condition, a 15% load increase, and a 15% load decrease.

1) Base Case Initial Loading Conditions: In this first case, the initial loading condition for each simulation is considered to be the same as the base case, i.e., the initial power flow of the regulated line is $P_{\text{line}}^0 = 55$ MW. This is also the reference power used for the HESS regulation.

We consider the case without HESS first. All the trajectories of P_{line} and their histogram and Probability Density Function (PDF) are calculated at $t = 20$ s, i.e., 5 seconds after the disturbance, as shown in Fig. 6. It can be seen how the fault, along with the variations of the wind and the load, can cause variations of P_{line} of up to ± 6.6 MW ($\pm 12\%$) after the transient.

A similar analysis is carried out considering a HESS in the system when both FES and BES are regulated by the PI controller (Fig. 7.a), the H_∞ controller (Fig. 7.b), and the combination of SM-H_∞ controllers (Fig. 7.c). From these figures, it can be observed how adding a HESS in the system can significantly reduce the variations of P_{line} by about 60-70%. Comparing the standard deviation of P_{line}, σ_P, the best performance is obtained when the SM control is applied to the FES, and the H_∞ control to the BES.

The total computational time to obtain all 1,000 trajectories for each case is: 18 m and 35 s for PI, 18 m and 45 s for H_∞, and 4 h and 15 m for SM and H_∞. The reason why the computational time when SM is included is so high compared to the other techniques is because SM high frequency switching requires a much smaller time step for the time domain simulations. While the first two controllers consider a time step of 0.02 s, the SM requires 0.004 s or

TABLE II: Comparison of σ_P and number of current saturations of the HESS controllers for different loading levels during a fault in the Irish system.

	No HESS	PI		H_∞		SM-H_∞	
Base Case (55.0 MW)							
σ_P [p.u.]	0.0219	0.0092	(-57.99%)	0.0083	(-62.10%)	0.0069	(-68.49%)
$n_{\text{sat FES}}$	-	75	-	1	(-98.67%)	103	$(+37.33\%)$
$n_{\text{sat BES}}$	-	269	-	116	(-56.88%)	51	(-81.04%)
15% Load Increase (63.25 MW)							
σ_P [p.u.]	0.0251	0.0110	(-56.18%)	0.0101	(-59.76%)	0.0093	(-62.95%)
$n_{\text{sat FES}}$	-	48	-	0	(-100.0%)	61	$(+27.08\%)$
$n_{\text{sat BES}}$	-	201	-	55	(-72.64%)	27	(-86.57%)
15% Load Decrease (46.75 MW)							
σ_P [p.u.]	0.0188	0.0079	(-57.98%)	0.0068	(-63.83%)	0.0059	(-68.62%)
$n_{\text{sat FES}}$	-	78	-	1	(-98.72%)	132	$(+69.23\%)$
$n_{\text{sat BES}}$	-	343	-	158	(-53.94%)	75	(-78.13%)
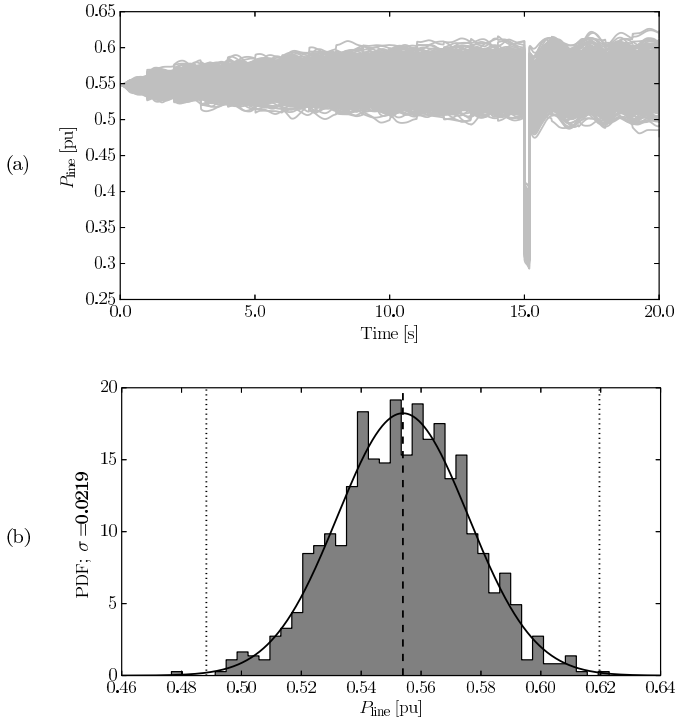
Fig. 6: Irish system without HESS and a three-phase fault followed by a line trip: Active power flowing through the regulated line. (a) All trajectories; (b) Histogram and PDF-fit of the trajectories at $t = 20$ s.

smaller. Also, SM needs a higher number of iterations to solve each point of the time integration method (the implicit trapezoidal method is used in this paper) whenever the SM switches its manifold. Clearly this numerical issue does not affect the actual implementation of the SM on the physical storage device.

2) Variations of the Initial Loading Conditions: The robustness of each controller is studied in this subsection considering different initial loading conditions, namely a 15% load increase ($P_{\text{line}}^0 = 63.25$ MW) and a 15% load decrease ($P_{\text{line}}^0 = 46.75$ MW). These are also the reference powers used for the HESS regulation for each case. For this study, the wind generation is assumed independent from the load variations, and therefore the power provided by the wind power plants remains the same for the three loading conditions. The power
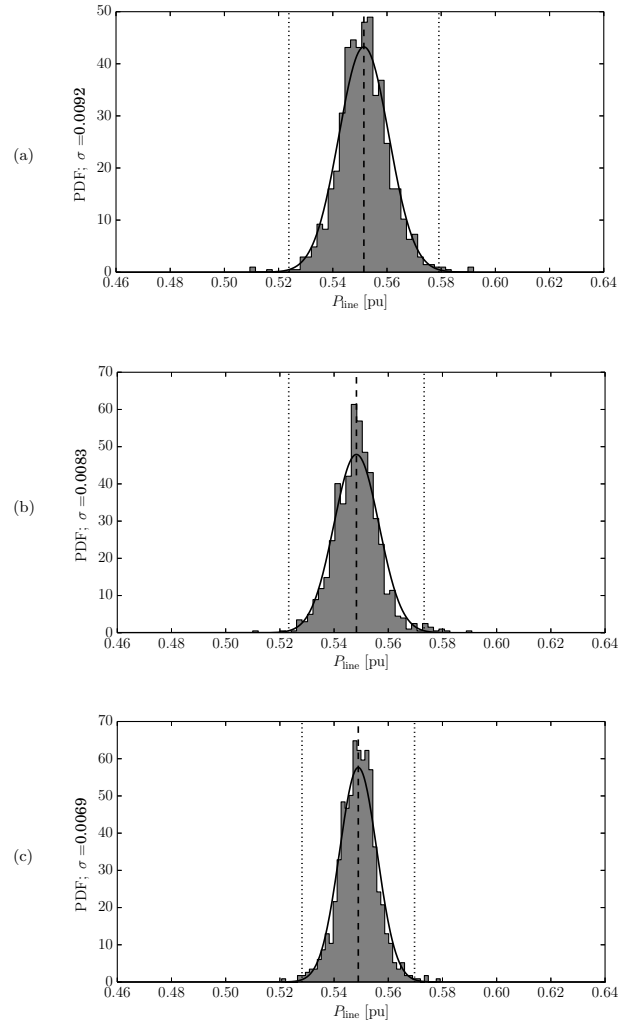
Fig. 7: Irish system with HESS and a three-phase fault followed by a line disconnection: Active power flowing through regulated line. (a) PI control; (b) H_∞ control; (c) SM-H_∞ control.

balance is kept by varying the power generated by the synchronous machines proportionally to the load variations. The same control parameters used for the base case are used for all control strategies. The standard deviation σ_P of the values

TABLE III: Comparison of σ_ω and $\Delta\mu_\omega$ for different HESS controllers during a synchronous machine outage in the Irish system.

	No HESS	PI		H$_\infty$		SM-H$_\infty$	
Before Loss of Sync. Machine							
σ_ω [Hz]	0.0124	0.0081	(-34.68%)	0.0079	(-36.29%)	0.0079	(-36.29%)
Frequency Nadir							
$\Delta\mu_\omega$ [Hz]	0.06	0.0415	(-30.83%)	0.03	(-50.00%)	0.035	(-41.67%)
σ_ω [Hz]	0.0125	0.0076	(-39.20%)	0.0067	(-46.40%)	0.007	(-44.00%)
After Loss of Sync. Machine							
σ_ω [Hz]	0.013	0.0081	(-37.69%)	0.0088	(-32.31%)	0.0079	(-39.23%)

of P_{line} and the number of trajectories for which the FES and the BES reach current saturations at $t = 20$ s for each of the three scenarios are listed in Table II.

The following are relevant remarks on the comparison of line active power flow regulation of the HESS from Table II:

- For all scenarios, the highest reduction of P_{line} variations is obtained when SM and H$_\infty$ are applied to the FES and BES, respectively.
- Comparing σ_P, the PI is the least sensitive to variations of the system loading level in terms of regulation capability.
- The PI has the highest probability of reaching current saturation of the HESS overall. The SM saturates the FES the most, since the effort to reach the sliding surface after a contingency is mainly taken by this device due to its fast response. On the other hand, the probability of the BES of reaching saturation in this case is the lowest in all scenarios. Finally, H$_\infty$ has the lowest probability of current saturations of the HESS overall. Note that the FES saturations in this case are very unlikely.
- Current saturations of the HESS are overall more likely for lower loading levels for all control strategies studied. As the initial loading level decreases, the overall inertia of the system is also reduced. This fact makes the system less resilient to large perturbations, which in turns results in higher variations of P_{line}, and thus, to a greater contribution of the HESS.

B. Primary Frequency Regulation

In this scenario, the system variable regulated by the HESS is the frequency of the bus that the storage device is connected to.[3] The contingency considered is the disconnection, at $t = 15$ s, of one of the synchronous machines of the system. The active power provided by the generation unit is 50 MW. Stochastic variations of both the wind speeds and the load power demands are also included in order to simulate system volatility in power production and consumption, respectively.

The same four cases discussed in subsection IV-A, namely no HESS, and with HESS applying PI, H$_\infty$, and SM-H$_\infty$ controllers, are considered. Also in this scenario, the PI regulator is initially tuned so to show a dynamic performance as similar as possible to the H$_\infty$ and SM. Then, 1,000 simulations are performed for each case, and the results of the standard deviations of the bus frequency, σ_ω, and the highest variation

[3]With this aim, the technique to estimate bus frequencies is the one proposed in [30].

of the frequency means, $\Delta\mu_\omega$, are listed in Table III for three conditions: right before the contingency, at the frequency nadir, and 10 s after the generation unit outage.

Several observations can be made based on Table III, as follows.

- Before the occurrence of the contingency, all controllers provide a fairly similar robustness against fluctuations of wind speeds and load powers.
- The highest reduction of both $\Delta\mu_\omega$ and σ_ω at the frequency nadir is obtained when applying H$_\infty$ control, followed by the combined SM-H$_\infty$ controller.
- The SM-H$_\infty$ strategy provides the best behavior 10 seconds after the loss of the synchronous machine, whereas the H$_\infty$ controller provides the poorest performance.

V. CONCLUSIONS

This paper describes and compares different ESS control strategies, namely PI, H$_\infty$ and SM. The formulations of these controllers are based on a generalized ESS model, and are duly defined and explained. The features of each control technique, as well as their main differences are also outlined. Finally, a comprehensive comparison of these control strategies is provided based on an exhaustive case study of the all-island Irish transmission system, with a HESS installed. The paper considers both line active power flow and primary frequency regulation provided by each controller for a large variety of scenarios, considering generation and load fluctuations.

Based on simulation results, the following conclusions can be drawn.

i. Overall, the most robust behavior of the HESS is achieved by applying the SM to the FES and the H$_\infty$ control to the BES. This combination is found to be the most effective to reduce both active power and frequency fluctuations. However, this approach shows the highest probability of current saturations of the FES.

ii. Applying H$_\infty$ to both FES and BES provides the lowest probability that current saturations will be experienced by the HESS. This approach provides also the highest reduction in frequency nadir variations after the loss of a synchronous machine. On the other hand, its performance is surpassed by the SM-H$_\infty$ controller for all other considered cases.

iii. While the dynamic performance of the PI control is overall the worst of the three techniques, it nevertheless shows a fair robustness against different loading conditions and contingencies, and system uncertainties. In

other words, the PI control provides a good trade-off between performance and simplicity of implementation and design. Therefore, the PI control can be used to provide a preliminary study of the behavior of the ESS in a power system, e.g., to check if the chosen location is the best one possible, and then H_∞ or SM control can be finally designed and applied to the ESS.

iv. Despite the deterministic nature of H_∞ and SM, all controllers have an heuristic component in their formulation and designs (gains of the PI regulator, K_u of the H_∞ controller, and K_{SMC} of the SM). These have to be carefully tuned to achieve an acceptable performance of the controllers. We think that this is an important practical remark that is seldom pointed out in the literature that describes robust control techniques.

This work can be extended in several different ways. We are currently working on studying the effectiveness of ESSs to provide secondary frequency control and we are exploring how to coordinate several storage devices with different primary controllers by means of a model predictive control approach. In the future, we will also focus on the impact of ESS devices on frequency, angle and voltage stability considering different storage technologies and controllers.

APPENDIX I
MODEL OF A FLYWHEEL ENERGY STORAGE

The model of the squirrel-cage induction machine proposed in [31] is used in this paper to model the FES. Using the generator convention, and the *dq*-frame representation, the voltages of the stator and rotor of the machine can be written as follows:

$$
\begin{aligned}
v_{ds} &= -R_s i_{ds} - \omega_s \psi_{qs} + \dot{\psi}_{ds} \\
v_{qs} &= -R_s i_{qs} + \omega_s \psi_{ds} + \dot{\psi}_{qs} \\
v_{dr} &= -R_r i_{dr} - \sigma_{sr}\omega_s \psi_{qr} + \dot{\psi}_{dr} = 0 \\
v_{qr} &= -R_r i_{qr} + \sigma_{sr}\omega_s \psi_{dr} + \dot{\psi}_{qr} = 0
\end{aligned}
\tag{14}
$$

where the subscripts s and r stand for stator and rotor variables, respectively; v, R and i are the machine voltage, resistance and current, respectively; ψ is the flux linkage; ω_s is the stator electrical frequency; and σ_{sr} is the rotor slip defined as:

$$
\sigma_{sr} = \frac{\omega_s - 0.5p\omega_r}{\omega_s}
\tag{15}
$$

with p the number of poles and ω_r the rotor speed of the machine.

The expressions of the flux linkages are given by:

$$
\begin{aligned}
\psi_{ds} &= -(L_s + L_m)i_{ds} - L_m i_{dr} \\
\psi_{qs} &= -(L_s + L_m)i_{qs} - L_m i_{qr} \\
\psi_{dr} &= -(L_r + L_m)i_{dr} - L_m i_{ds} \\
\psi_{qr} &= -(L_r + L_m)i_{qr} - L_m i_{qs}
\end{aligned}
\tag{16}
$$

where L_s, L_r and L_m are the stator, rotor and mutual inductances, respectively.

The mechanical equations of the induction machine are the following:

$$
\begin{aligned}
T_e &= \psi_{dr}i_{qr} - \psi_{qr}i_{dr} \\
H_{FES}\dot{\omega}_r &= (T_m - T_e) - D_{FES}\omega_r
\end{aligned}
\tag{17}
$$

with T_e and T_m the electromechanical and mechanical torques, respectively; and H_{FES} and D_{FES} the inertia constant and rotor damping of the FES.

The active and reactive powers generated/absorbed by the machine are defined by:

$$
\begin{aligned}
P_{FES} &= v_{ds}i_{ds} + v_{qs}i_{qs} \\
Q_{FES} &= v_{qs}i_{ds} - v_{ds}i_{qs}
\end{aligned}
\tag{18}
$$

An ac/dc converter is used to connect, through its current output i_{dc}, the flywheel device with the dc side of the VSC. The converter is modeled in a similar way as the VSC described in [13].

Finally, the actual energy stored in the FES can be computed as follows:

$$
E_{FES} = H_{FES}\omega_r^2
\tag{19}
$$

Applying the notation of the GEM above to the FES, one has:

$$
\begin{aligned}
\boldsymbol{x} &= [\omega_r \; T_e]^T; \; \boldsymbol{z} = [v_{ds} \; v_{qs} \; v_{dr} \; v_{qr} \; \ldots]^T; \; u = \omega_s; \\
\boldsymbol{\rho} &= [H_{FES} \; 0]; \; \boldsymbol{\beta} = [2 \; 1]; \; \boldsymbol{\chi} = [0 \; 0]
\end{aligned}
\tag{20}
$$

where the dots in $\boldsymbol{z}$ stand for the stator and rotor currents and flux leakages, and the ac/dc converter variables.

APPENDIX II
MODEL OF A BATTERY ENERGY STORAGE [13]

A commonly-used model to represent the dynamics of a rechargeable battery cell is the Shepherd model [32]:

$$
\begin{aligned}
\dot{Q}_e &= i_b/3600 \\
\dot{i}_m &= \frac{i_b - i_m}{T_m} \\
0 &= v_{oc} - v_p(Q_e, i_m) + v_e e^{-\beta_e Q_e} - R_i i_b - v_b
\end{aligned}
\tag{21}
$$

where Q_e is the extracted capacity in Ah; i_m is the battery current i_b passed through a low-pass filter with time constant T_m; v_{oc}, v_p and v_e are the open-circuit, polarization and exponential voltages, respectively; β_e is the exponential zone time constant inverse; R_i is the internal battery resistance; and v_b is the battery voltage.

The variation of the polarization voltage v_p with respect to i_m and Q_e is given by:

$$v_{\mathrm{p}}(Q_{\mathrm{e}}, i_{\mathrm{m}}) = \begin{cases} \dfrac{R_{\mathrm{p}} i_{\mathrm{m}} + K_{\mathrm{p}} Q_{\mathrm{e}}}{\mathrm{SOC}} & \text{if} \quad i_{\mathrm{m}} > 0 \ \text{(discharge)} \\[2mm] \dfrac{R_{\mathrm{p}} i_{\mathrm{m}}}{q_{\mathrm{e}} + 0.1} + \dfrac{K_{\mathrm{p}} Q_{\mathrm{e}}}{\mathrm{SOC}} & \text{if} \quad i_{\mathrm{m}} \leq 0 \ \text{(charge)} \end{cases}$$

$$(22)$$

where R_{p} and K_{p} are the polarization resistant and polarization constant, respectively; and SOC is the state of charge of the battery which is defined as:

$$\mathrm{SOC} = \frac{Q_{\mathrm{n}} - Q_{\mathrm{e}}}{Q_{\mathrm{n}}} = 1 - q_{\mathrm{e}} \qquad (23)$$

The non-linearity of v_{p} implies that depending on the state of the battery (charge or discharge), two different sets of equations can be obtained by applying the GEM. Therefore, the GEM has to be able to switch from one set to another depending on the BES operation.

The connection of the BES to the VSC is given by:

$$\begin{aligned} 0 &= (1 - 2S) v_{\mathrm{dc}} - n_{\mathrm{s}} v_{\mathrm{b}} \\ i_{\mathrm{dc}} &= -(1 - 2S) n_{\mathrm{p}} i_{\mathrm{b}} \end{aligned} \qquad (24)$$

where S is the duty cycle of the battery dc/dc converter; and n_{p} and n_{s} are the number of parallel and series connected battery cells, respectively. The dc/dc converter connection used in this paper is based on [33].

Imposing the GEM to BES equations, one has:

$$\boldsymbol{x} = [Q_{\mathrm{e}} \ v_{\mathrm{b}}]^T; \ \boldsymbol{z} = [i_{\mathrm{b}} \ i_{\mathrm{m}} \ v_{\mathrm{p}}]^T; \ u = S;$$

$$\boldsymbol{\rho} = \left[-\frac{1}{Q_{\mathrm{n}}} \ 0 \right]; \ \boldsymbol{\beta} = [1 \ 1]; \ \boldsymbol{\chi} = [Q_{\mathrm{n}} \ 0]. \qquad (25)$$

References

[1] H. Ibrahim, A. Ilinca, and J. Perron, "Energy Storage Systems - Characteristics and Comparisons," *Renewable and Sustainable Energy Reviews*, vol. 12, pp. 1221–1250, 2008.

[2] M. Beaudin, H. Zareipour, A. Schellenberglabe, and W. Rosehart, "Energy Storage for Mitigating the Variability of Renewable Electricity Sources: An Updated Review," *Energy for Sustainable Development*, vol. 14, pp. 302–313, 2010.

[3] M. G. Molina, P. E. Mercado, and E. H. Watanabe, "Improved Superconducting Magnetic Energy Storage (SMES) Controller for High-Power Utility Applications," *IEEE Transactions on Energy Conversion*, vol. 26, no. 2, pp. 444 – 456, June 2011.

[4] G. Li, S. Cheng, J. Wen, Y. Pan, and J. Ma, "Power System Stability Enhancement by a Double-fed Induction Machine with a Flywheel Energy Storage System," in *Proceedings of the Power Engineering Society General Meeting, IEEE*, Montreal, Que, 2006.

[5] V. P. Singh, S. R. Mohanty, N. Kishor, and P. K. Ray, "Robust H-infinity load frequency control in hybrid distributed generation system," *Electrical Power & Energy Systems*, vol. 46, pp. 294–305, 2013.

[6] D. Zhu and G. Hug-Glanzmann, "Robust Control Design for Integration of Energy Storage into Frequency Regulation," in *Proceedings of the Innovative Smart Grid Technologies (ISGT Europe), 3rd IEEE PES International Conference and Exhibition*, Berlin, Oct. 2012, pp. 1–8.

[7] F. A. Inthamoussou, J. Pegueroles-Queralt, and F. D. Bianchi, "Control of a Supercapacitor Energy Storage System for Microgrid Applications," *IEEE Transactions on Energy Conversion*, vol. 28, no. 3, pp. 690–697, Sept. 2013.

[8] D. Kairous and R. Wamkeue, "DFIG-Based Fuzzy Sliding-Mode Control of WECS With a Flywheel Energy Storage," *Electric Power System Research*, vol. 93, pp. 16–23, Dec. 2012.

[9] A. Etxeberria, I. Vechiu, H. Camblong, and J.-M. Vinassa, "Comparison of Sliding Mode and PI Control of a Hybrid Energy Storage System in a Microgrid Application," in *Proceedings of the International Conference on Smart Grid and Clean Energy Technologies*, Chengdu, China, Sept. 2011, pp. 966–974.

[10] T. D. Nguyen, K. J. Tseng, S. Zhang, S. Zhang, and H. T. Nguyen, "Model Predictive Control of a Novel Axial Flux Permanent Magnet Machine for Flywheel Energy Storage System," in *IPEC, 2010 Conference Proceedings*, Oct 2010, pp. 519–524.

[11] C. Trabert, A. Ulbig, and G. Andersson, "Model Predictive Frequency Control employing stability constraints," in *Proceedings of the American Control Conference (ACC), 2015*, July 2015, pp. 5678–5685.

[12] K. Zhang, C. Mao, J. Lu, D. Wang, X. Chen, and J. Zhang, "Optimal Control of State-of-Charge of Superconducting Magnetic Energy Storage for Wind Power System," *IET Renewable Power Generation*, vol. 8, no. 1, pp. 58–66, Jan. 2014.

[13] Á. Ortega and F. Milano, "Generalized Model of VSC-based Energy Storage Systems for Transient Stability Analysis," *IEEE Transactions on Power Systems*, 2016, (in press).

[14] ——, "Comparison of Different Control Strategies for Energy Storage Devices," in *Proceedings of the Power System Computation Conference (PSCC)*, Genoa, Italy, June 2016, (accepted for publication). [Online]. Available: http://faraday1.ucd.ie/archive/papers/esscontrol.pdf

[15] F. Milano and R. Zárate-Miñano, "A Systematic Method to Model Power Systems as Stochastic Differential Algebraic Equations," *IEEE Transactions on Power Systems*, vol. 28, no. 4, pp. 4537–4544, Nov. 2013.

[16] N. R. Chaudhuri, B. Chauduri, R. Majumder, and A. Yazdani, *Multiterminal Direct-current Grids: Modeling, Analysis, and Control*. John Wiley & Sons, 2014.

[17] F. Milano, "Semi-Implicit Formulation of Differential-Algebraic Equations for Transient Stability Analysis," *IEEE Transactions on Power Systems*, vol. PP, no. 99, pp. 1–10, 2016.

[18] Á. Ortega and F. Milano, "Design of a Control Limiter to Improve the Dynamic Response of Energy Storage Systems," in *Proceedings of the Power Engineering Society General Meeting, IEEE*, Denver, Colorado, USA, July 2015.

[19] S. P. Bhattacharyya, H. Chapellat, and L. H. Keel, *Robust Control: The Parametric Approach*. Prentice Hall, June 1995, ch. 13.

[20] P. Benner, V. Mehrmann, V. Sima, S. Van Huffel, and A. Varga, "SLICOT – A Subroutine Library in Systems and Control Theory," *Applied and Computational Control, Signal and Circuits*, vol. 1, no. 10, pp. 499–539, Nov. 1999.

[21] V. Utkin, J. Guldner, and J. Shi, *Sliding Mode Control in Electro-Mechanical Systems*, 2nd ed. CRC Press, 2009.

[22] R. Zárate-Miñano and F. Milano, "Construction of SDE-based Wind Speed Models with Exponentially Decaying Autocorrelation," *Renewable Energy*, Mar. 2016, (in press). [Online]. Available: http://faraday1.ucd.ie/archive/papers/windsde2.pdf

[23] D. T. Gillespie, "Exact Numerical Simulation of the Ornstein-Uhlenbeck Process and its Integral," *Physical Review E*, vol. 54, no. 2, pp. 2084–2091, 1996.

[24] M. Perninge, V. Knazkins, M. Amelin, and L. Söder, "Risk Estimation of Critical Time to Voltage Instability Induced by Saddle-Node Bifurcation," *IEEE Transactions on Power Systems*, vol. 25, no. 3, pp. 1600–1610, Aug. 2010.

[25] Schwungrad Energie Limited, "Rhode Hybrid Energy Storage Test Facility," URL: http://schwungrad-energie.com/projects/rhode-hybrid-test-facility/.

[26] EirGrid Group, "All Island Irish Transmission System Map," URL: http://smartgriddashboard.eirgrid.com/#all/transmission-map.

[27] Schwungrad Energie Limited, "First Hybrid-Flywheel Energy Storage Plant in Europe Announced in Ireland," URL: http://schwungrad-energie.com/hybrid-flywheel-energy-storage-plant-europe-announced-ireland/.

[28] Department of Jobs, Enterprise and Innovation, Ireland, "First Hybrid-Flywheel Energy Storage Plant in Europe Announced in Ireland," URL: https://www.djei.ie/en/News-And-Events/Department-News/2015/March/First-Hybrid-Flywheel-Energy-Storage-Plant-in-Europe-announced-in-Midlands-.html.

[29] F. Milano, "A Python-based Software Tool for Power System Analysis," in *Procs. of the IEEE PES General Meeting*, Vancouver, BC, July 2013.

[30] F. Milano and Á. Ortega, "Frequency Divider," *IEEE Transactions on Power Systems*, 2016, (in press). [Online]. Available: http://faraday1.ucd.ie/archive/papers/freqdiv.pdf

[31] P. C. Krause, O. Wasynczuk, and S. D. Sudhoff, *Analysis of Electric Machinery and Drive Systems*, 3rd ed. Wiley-IEEE Press, 2013.

[32] C. M. Shepherd, "Design of Primary and Secondary Cells II. An Equation Describing Battery Discharge," *Journal of the Electrochemical Society*, vol. 112, no. 7, pp. 657–664, 1965.

[33] A. Esmaili, B. Novakovic, A. Nasiri, and O. Abdel-Baqi, "A Hybrid System of Li-Ion Capacitors and Flow Battery for Dynamic Wind Energy Support," *IEEE Transactions on Industry Applications*, vol. 49, no. 4, pp. 1649–1657, Aug. 2013.

Federico Milano (S'02, M'04, SM'09, F'16) received from the Univ. of Genoa, Italy, the ME and Ph.D. in Electrical Eng. in 1999 and 2003, respectively. From 2001 to 2002 he was with the Univ. of Waterloo, Canada, as a Visiting Scholar. From 2003 to 2013, he was with the Univ. of Castilla-La Mancha, Spain. In 2013, he joined the Univ. College Dublin, Ireland, where he is currently Professor of Power Systems Control and Protections. His research interests include power system modeling, stability analysis and control.

Álvaro Ortega (S'14) received from Escuela Superior de Ingenieros Industriales, University of Castilla-La Mancha, Ciudad Real, Spain, the degree in Industrial Engineering in 2013. Since September 2013, he is a Ph.D. student candidate with the Electricity Research Center, University College Dublin, Ireland. His current research interests are in the dynamic modeling, control and stability of energy storage systems connected to transmission and distribution systems.